PROCEEDINGS OF SCIENCE

ONLINE ICRC 2021
THE ASTROPARTICLE PHYSICS CONFERENCE
Berlin | Germany
37th International Cosmic Ray Conference
12–23 July 2021

Simulating cosmic rays and the gamma-ray emission in star-forming galaxies

Maria Werhahn,[a,b,*] **Christoph Pfrommer**[a] **and Philipp Girichidis**[a]

[a] *Leibniz-Institut für Astrophysik Potsdam (AIP),*
An der Sternwarte 16, 14482 Potsdam, Germany
[b] *Universität Potsdam, Institut für Physik und Astronomie,*
Karl-Liebknecht-Str. 24/25, 14476 Golm, Germany
E-mail: mwerhahn@aip.de

Previously, the non-thermal emission from galaxies has only been modeled with parametrized 1D or 2D models, which is insufficient to explain a multitude of new, spatially resolved multi-messenger data of cosmic ray (CR) spectra, at gamma-rays and in the radio. Instead, we perform high-resolution magneto-hydrodynamic simulations of galaxies using the moving mesh code AREPO with self-consistent CR physics. In post-processing, we calculate steady-state spectra of CRs including all relevant cooling and escape losses. Consistent with Voyager-1 and AMS-02 data, our models show a turn-over of proton spectra below GeV energies due to Coulomb interactions so that electrons start to dominate the total particle spectra and match the shape of the positron fraction up to 10 GeV. Furthermore, from our CR spectra, we calculate multi-frequency spectra, from the radio up to the TeV energy regime, due to all non-thermal emission processes, i.e. synchrotron, bremsstrahlung, inverse Compton (IC) emission and gamma-ray emission from neutral pion decay. This allows us to produce detailed emission maps, luminosities and spectra of our simulated galaxies, that range from dwarfs to Milk-Way analogues to starburst galaxies, at different evolutionary stages. Within our simulations, we can successfully reproduce the observed far infrared (FIR)-gamma-ray and FIR-radio relations. We find that highly SF galaxies are close to the calorimetric limit and hence, their gamma-ray emission is dominated by neutral pion decay. However, in low SF galaxies, escape losses due to diffusion steepen the spectra and in turn, an increasing contribution from IC emission is needed to reproduce the observed gamma-ray spectra.

37th International Cosmic Ray Conference (ICRC 2021)
July 12th – 23rd, 2021
Online – Berlin, Germany

*Presenter

PoS(ICRC2021)665

1. Introduction

The importance of CRs in the evolution of star-forming galaxies has been shown in various simulations [e.g. 1–4]. The different approaches of CR modeling can be constrained by comparing the non-thermal emission arising from CRs with observations, ranging from radio frequencies up to high-energy gamma-rays. The former is produced by primary and secondary CR electrons, that emit synchrotron radiation in the presence of a galactic magnetic field. In the gamma-ray regime, CR electrons contribute via bremsstrahlung and IC emission, whereas CR protons collide with particles in the interstellar medium (ISM), producing pions that decay further into gamma-ray photons (if the pions are neutrally charged) or secondary electrons or positrons (if the pions are negatively or positively charged, respectively).

The modeling of non-thermal emission from nearby star-forming galaxies has been done via the adaption of one-zone models, 1D flux tube or 2D axisymmetric models, where the relevant physical quantities of the galaxies are considered as free parameters in order to match the observations [e.g. 5–7]. We present a different approach in three previously published papers [8, 9] and [10], where we perform 3D magneto-hydrodynamical (MHD) simulations with the moving mesh code AREPO [11, 12] of the formation of isolated galaxies that reside in dark matter halos with masses ranging from $M_{200} = 10^{10}$ to $10^{12}\,\mathrm{M}_\odot$ and follow the evolution of CR protons self-consistently. Starting from a gas cloud in hydrostatic equilibrium, that collapses as a consequence of cooling, our simulations exhibit an initial burst of star-formation, that subsequently declines exponentially. At remnants of SN explosions, CRs are injected with efficiencies of $\zeta_{\mathrm{SN}} = 0.05$ or 0.10, mimicking the acceleration of CRs at the shocks of SN explosions due to diffusive shock acceleration. CRs are then modeled via the two-moment description and are advected with the gas in our 'CR adv' model, whereas they additionally diffuse anisotropically along magnetic field lines in the 'CR diff' model with a diffusion coefficient parallel to the magnetic field of $D = 10^{28}\,\mathrm{cm}^2/\mathrm{s}$. This enables us to pinpoint the effect of different CR transport models within our simulations on observable quantities. In the following, we summarize our modeling of the CR spectra and non-thermal emission processes and provide the main results, that are detailed in [8], [9] and [10].

2. Cosmic ray spectra

In order to model the spectral energy distributions of CR protons, primary and secondary electrons, we assume a steady-state in every computational cell and calculate the resulting equilibrium spectra for each CR population. We account for hadronic losses and Coulomb cooling for CR protons, whereas CR electrons lose energy due to synchrotron, IC and bremsstrahlung emission, in addition to Coulomb losses. As an incident radiation field for IC scattering, we take the CMB and an UV photon field into account, where the latter is assumed to be absorbed by dust and re-emitted in the FIR. Furthermore, we calculate escape losses due to advection and diffusion, where we adapt an energy dependent diffusion coefficient for the latter, $D \propto E^{\delta}$. The production of secondary electrons and positrons (hereafter secondary electrons) is calculated by adapting various descriptions of the cross sections of pion production from the literature [13, 14] and interpolating in the intermediate energy regime of the kinetic energy of CR protons [8].

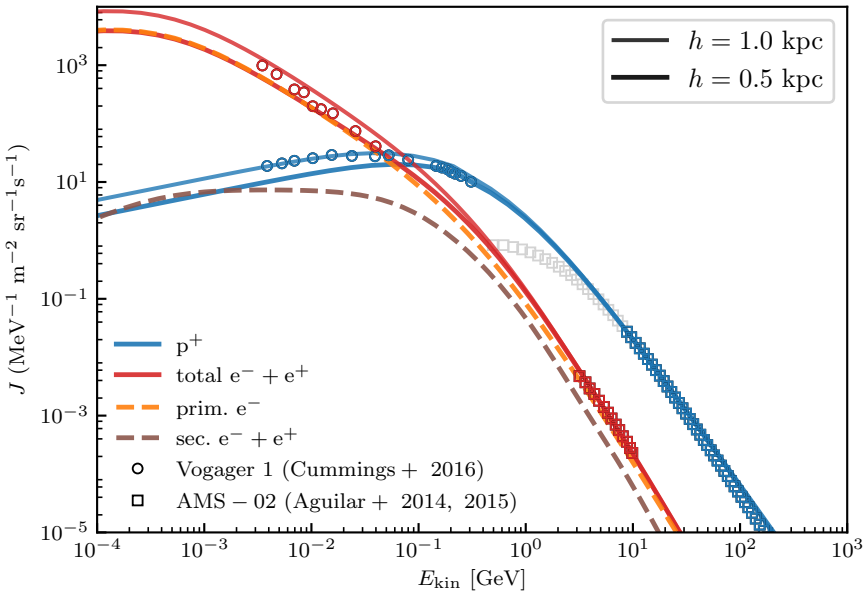

Figure 1: CR proton (blue) and electron (red) spectra as observed by Voyager 1 [15] (circles) and AMS-02 [16, 17] (squares). The data below 1 GeV of AMS-02 that is affected by solar modulation is shown in grey. The solid lines show the CR spectra from [8] of a simulated Milky Way-like galaxy averaged in annuli with a radius of $7 < r < 9$ kpc and a height above and below the mid-plane of $h = 1.0$ and 0.5 kpc, as indicated in the legend. The orange and brown lines show the contribution of primary and secondary electrons to the total electron spectrum, respectively.

In Fig. 1 we show the CR spectra of a Milky Way-like galaxy (i.e. with a similar halo mass and SFR, i.e. $M_{200} = 10^{12}\,\mathrm{M}_\odot$ and $\dot{M}_\star = 1.7\,\mathrm{M}_\odot\,\mathrm{yr}^{-1}$), averaged over a ring around the solar-galactic radius ($7 < r < 9$ kpc) and different heights h as denoted in the legend. Intriguingly, without further tweaking of the parameters, we match the observed inversion of the CR spectra at low energies: whereas at high energies, CR protons dominate the total spectrum, they turn over at ~ 1 GeV and are hence exceeded by CR electrons. We find that this is due to Coulomb losses, that shape the spectra at low energies [8]. The ratio of the steady-state spectra of CR protons to electrons scales as $f_\mathrm{p}/f_\mathrm{e} \propto \beta_\mathrm{p}/\beta_\mathrm{e}$, where $\beta_\mathrm{e/p} = v_\mathrm{e/p}/c$ denotes the normalised velocities of electrons and protons, respectively. Consequently, with decreasing kinetic energies, CR protons experience a suppression when becoming non-relativistic, i.e. at around 1 GeV, in contrast to CR electrons, that only become non-relativistic at much lower energies, due to their lower rest mass energy [8]. Additionally, our models are able to reproduce the observed decreasing positron fraction up to 8 GeV [8]. This corroborates the robustness of our modeling of CR transport in galaxies, which is the starting point for the analysis of the resulting non-thermal emission processes.

3. Gamma-ray emission

From the equilibrium spectra of CR protons, we calculate the production of gamma-ray emission due to neutral pion decay, in addition to IC and bremsstrahlung emission from primary and secondary

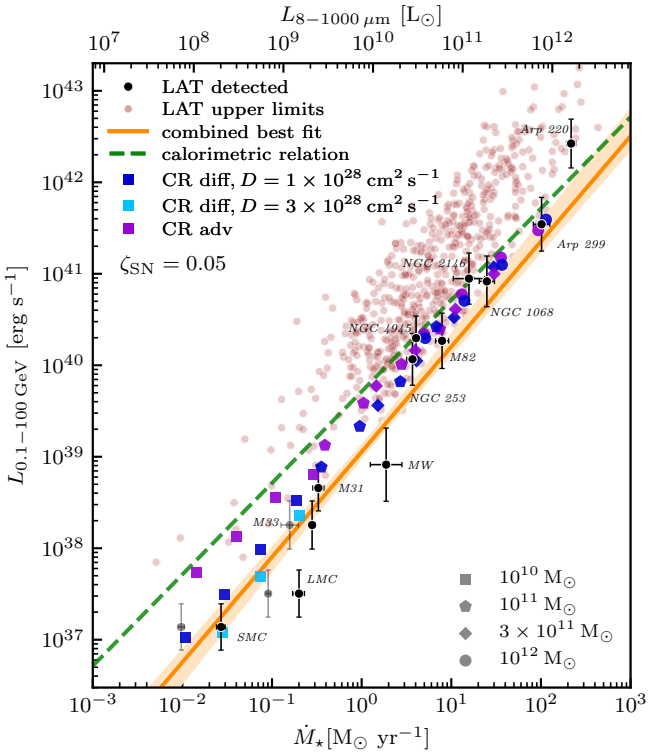

Figure 2: FIR-γ-ray relation as shown in [9]: our simulations with $\zeta_{SN} = 0.05$ and different halo masses (represented by different symbols as indicated in the legend) match the observed relation by [18] if we include CR diffusion (dark blue symbols), whereas only accounting for CR advection (purple symbols) over-predicts the observations, which deviate from the calorimetric relation (green dashed line) towards smaller SFRs. Increasing the diffusion coefficient decreases the gamma-ray luminosities further towards smaller SFRs (light blue symbols). The SFR of the simulated galaxies (lower axis) are converted to a FIR-luminosity (upper axis) by adapting the Kennicutt law [19]. For the SMC, LMC and M33, we show in addition to their FIR-luminosities (grey symbols) their SFRs (black symbols, see [9] for details).

CR electrons. This allows us to calculate total gamma-ray luminosities and produce detailed maps and spectra of our simulated star-forming galaxies across all halo masses and evolutionary stages. Due to the initial starburst after the collapse of the gas cloud and the exponentially declining SFR, our simulations cover a broad range in SFRs and populate the FIR-gamma-ray relation from 10^{-2} to $10^2\,M_\odot\,yr^{-1}$ in Fig. 2. By adapting an injection efficiency of $\zeta_{SN} = 0.05$, we successfully match the observed relation in our 'CR diff' model [9]. This included the observed deviation from the calorimetric relation at low SFRs, where diffusive losses become increasingly more relevant [9]. Hence, the model that only accounts for CR advection over-predicts the observed gamma-ray luminosities at low SFRs. This also affects the shapes of the gamma-ray spectra that steepen with the increasing relevance of diffusive losses with decreasing SFR. However, in our model, this is partly compensated by IC emission that hardens the spectra at high frequencies [9]. Furthermore, a comparison of famous starburst galaxies like M82, NGC 253 and NGC 2146 with snapshots of our simulation that exhibit similar SFRs and gamma-ray luminosities shows that a shallower energy-dependent diffusion coefficient $D \propto E^{0.3}$ is in better agreement with the observations than adapting

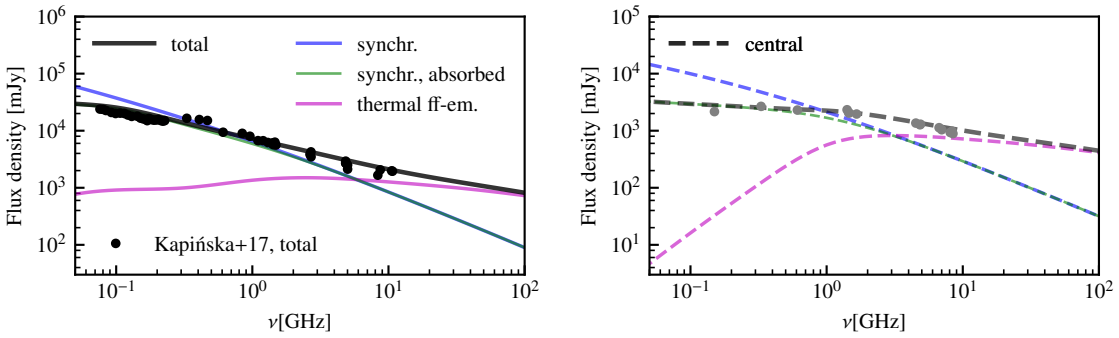

Figure 3: Radio spectrum from [10]: the radio synchrotron spectrum (blue line) from a simulation with a similar SFR and total radio luminosity as NGC 253 is shown together with the total observed radio spectrum in the left-hand panel (black points, [20]), whereas the right-hand panel shows the central region with a radius of 150 pc (grey points and dashed lines). Free-free absorption flattens the synchrotron spectra towards small frequencies (green solid and dashed lines) and a contribution from thermal free-free emission hardens the radio spectra towards higher frequencies (magenta line). See [10] for details of the calculation of the spectra.

the scaling as observed in the Milky Way, i.e. $D \propto E^{0.5}$ [9]. However, more data in particular at high energies above 100 GeV is needed in order to better constrain the transport of CRs in various SF environments.

4. Radio emission

Complementary to our study of CR spectra and gamma-ray emission from star-forming galaxies in [8] and [9], we analyse the radio emission from our simulated galaxies in [10]. We find that the FIR-radio correlation is reproduced with our simulations in the CR diff model, where the total radio luminosity is dominated by primary emission (see Fig. 4). This is due diffusive losses of CR protons that suppress the efficient production of secondary electrons and steepen their spectra, which leads to steeper secondary CR electron spectra compared to primary electrons and hence a smaller contribution from secondaries to the total radio emission [10].

One of the implications of calorimetric theory, i.e. that CR electrons lose most of their energy due to IC and synchrotron emission, is the occurrence of steep radio spectra: if IC and synchrotron cooling dominate, the steady-state spectra of CR electrons would be steepened by 1 compared to the injected spectrum, i.e $\alpha_\mathrm{e} = \alpha_\mathrm{inj} - 1$, since these losses scale with energy as $\tau_\mathrm{IC/syn} \propto E^{-1}$. This results in spectral indices of $\alpha_\nu = (\alpha_\mathrm{e} - 1)/2 \approx 1.1$ for typical injected spectral indices of $\alpha_\mathrm{inj} = 2.2$, which contradicts the observed flat radio spectra with $\alpha_\nu = 0.5$ to 0.8.

One possibility to maintain or flatten the CR electron and hence the resulting radio spectra would be if bremsstrahlung or Coulomb losses played an important role compared to other losses due to their different energy dependence. However, we find that these losses only dominate at low electron energies and hence can not be responsible for the observed flat radio spectra in particular at high frequencies [10]. Instead, the inclusion of a thermal component, i.e. the emission due to thermal free-free interactions of CR electrons with free electrons in the ISM, hardens the spectra at high frequencies [10, 22] (see Fig. 3). In addition, free-free absorption flattens the spectra at

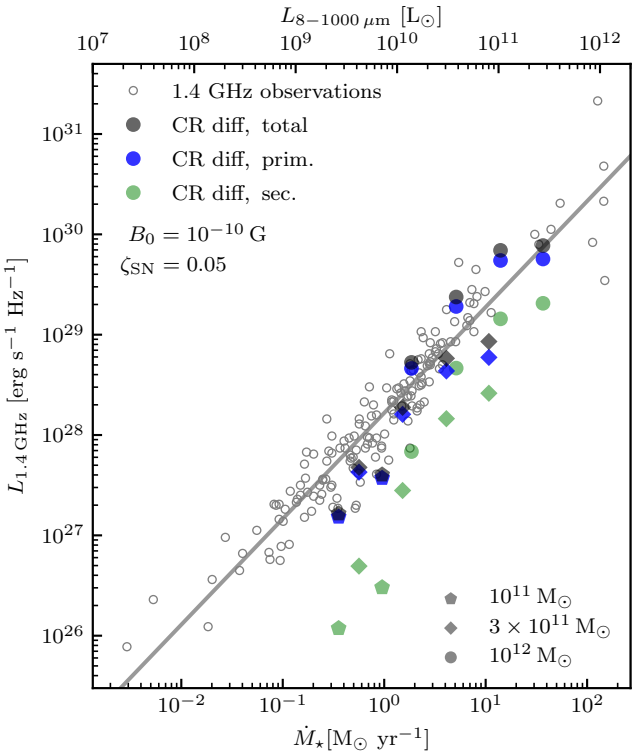

Figure 4: FIR-radio correlation as shown in [10]. The contributions to the total face-on radio luminosities from our simulations adapting the 'CR diff' model (black symbols) from primary (blue symbols) and secondary electrons (green symbols) are shown separately. The symbols correspond to different halo masses of our simulations as shown in the lower right. The grey line represents a fit to the data by [21] (open circles).

low frequencies, which has been observed to be particularly strong towards the central regions of starburst galaxies like NGC 253 [10, 20]. This finding enables us to reconcile calorimetric theory with observations.

5. Summary

The modeling of steady-state CR proton and electron spectra in 3D MHD simulations enabled us to gain new insights into the underlying physical processes that are responsible for the observed relations between non-thermal radio and gamma-ray emission with tracers of SF in galaxies. Possible improvements of this model would be cosmological simulations in order to obtain a more realistic SF history, as well as the inclusion of full spectral-dynamical simulations of CRs [23, 24]. Furthermore, future improvements of the ISM model might enable us to resolve the turbulence induced by SF, potentially yielding a stronger magnetic large-scale dynamo.

References

[1] M. Jubelgas, V. Springel, T. Enßlin and C. Pfrommer, *Cosmic ray feedback in hydrodynamical simulations of galaxy formation*, *A&A* **481** (2008) 33 [astro-ph/0603485].

[2] M. Salem and G.L. Bryan, *Cosmic ray driven outflows in global galaxy disc models*, *MNRAS* **437** (2014) 3312 [1307.6215].

[3] R. Pakmor, C. Pfrommer, C.M. Simpson and V. Springel, *Galactic Winds Driven by Isotropic and Anisotropic Cosmic-Ray Diffusion in Disk Galaxies*, *ApJ* **824** (2016) L30 [1605.00643].

[4] S. Jacob, R. Pakmor, C.M. Simpson, V. Springel and C. Pfrommer, *The dependence of cosmic ray-driven galactic winds on halo mass*, *MNRAS* **475** (2018) 570 [1712.04947].

[5] D.F. Torres, *Theoretical Modeling of the Diffuse Emission of Gamma Rays from Extreme Regions of Star Formation: The Case of ARP 220*, *ApJ* **617** (2004) 966 [astro-ph/0407240].

[6] B.C. Lacki, T.A. Thompson and E. Quataert, *The Physics of the Far-infrared-Radio Correlation. I. Calorimetry, Conspiracy, and Implications*, *ApJ* **717** (2010) 1 [0907.4161].

[7] T.M. Yoast-Hull, J.E. Everett, I. Gallagher, J. S. and E.G. Zweibel, *Winds, Clumps, and Interacting Cosmic Rays in M82*, *ApJ* **768** (2013) 53 [1303.4305].

[8] M. Werhahn, C. Pfrommer, P. Girichidis, E. Puchwein and R. Pakmor, *Cosmic rays and non-thermal emission in simulated galaxies – I. Electron and proton spectra compared to Voyager-1 data*, *MNRAS* **505** (2021) 3273 [https://academic.oup.com/mnras/article-pdf/505/3/3273/38659223/stab1324.pdf].

[9] M. Werhahn, C. Pfrommer, P. Girichidis and G. Winner, *Cosmic rays and non-thermal emission in simulated galaxies – II. γ-ray maps, spectra, and the far-infrared–γ-ray relation*, *MNRAS* **505** (2021) 3295 [https://academic.oup.com/mnras/article-pdf/505/3/3295/38659066/stab1325.pdf].

[10] M. Werhahn, C. Pfrommer and P. Girichidis, *Cosmic rays and non-thermal emission in simulated galaxies: III. probing cosmic ray calorimetry with radio spectra and the FIR-radio correlation*, *subm.* (2021) [2105.12134].

[11] V. Springel, *E pur si muove: Galilean-invariant cosmological hydrodynamical simulations on a moving mesh*, *MNRAS* **401** (2010) 791 [0901.4107].

[12] R. Pakmor, V. Springel, A. Bauer, P. Mocz, D.J. Munoz, S.T. Ohlmann et al., *Improving the convergence properties of the moving-mesh code AREPO*, *MNRAS* **455** (2016) 1134 [1503.00562].

[13] S.R. Kelner, F.A. Aharonian and V.V. Bugayov, *Energy spectra of gamma rays, electrons, and neutrinos produced at proton-proton interactions in the very high energy regime*, *Phys. Rev. D* **74** (2006) 034018 [astro-ph/0606058].

[14] R.-z. Yang, E. Kafexhiu and F. Aharonian, *Exploring the shape of the γ-ray spectrum around the "π^0-bump"*, *A&A* **615** (2018) A108 [1803.05072].

PoS(ICRC2021)665

[15] A.C. Cummings, E.C. Stone, B.C. Heikkila, N. Lal, W.R. Webber, G. Jóhannesson et al., *Galactic cosmic rays in the local interstellar medium: Voyager 1 observations and model results*, *The Astrophysical Journal* **831** (2016) 18.

[16] AMS collaboration, *Electron and positron fluxes in primary cosmic rays measured with the alpha magnetic spectrometer on the international space station*, *Phys. Rev. Lett.* **113** (2014) 121102.

[17] M. Aguilar, D. Aisa, B. Alpat, A. Alvino, G. Ambrosi, K. Andeen et al., *Precision Measurement of the Proton Flux in Primary Cosmic Rays from Rigidity 1 GV to 1.8 TV with the Alpha Magnetic Spectrometer on the International Space Station*, *Phys. Rev. Lett.* **114** (2015) 171103.

[18] P. Kornecki, L.J. Pellizza, S. del Palacio, A.L. Müller, J.F. Albacete-Colombo and G.E. Romero, *γ-ray/infrared luminosity correlation of star-forming galaxies*, *A&A* **641** (2020) A147 [2007.07430].

[19] R.C. Kennicutt, Jr., *Star Formation in Galaxies Along the Hubble Sequence*, *ARA&A* **36** (1998) 189 [astro-ph/9807187].

[20] A.D. Kapińska, L. Staveley-Smith, R. Crocker, G.R. Meurer, S. Bhandari, N. Hurley-Walker et al., *Spectral Energy Distribution and Radio Halo of NGC 253 at Low Radio Frequencies*, *ApJ* **838** (2017) 68 [1702.02434].

[21] E.F. Bell, *Estimating Star Formation Rates from Infrared and Radio Luminosities: The Origin of the Radio-Infrared Correlation*, *ApJ* **586** (2003) 794 [astro-ph/0212121].

[22] E. Peretti, P. Blasi, F. Aharonian and G. Morlino, *Cosmic ray transport and radiative processes in nuclei of starburst galaxies*, *MNRAS* **487** (2019) 168 [1812.01996].

[23] P. Girichidis, C. Pfrommer, M. Hanasz and T. Naab, *Spectrally resolved cosmic ray hydrodynamics - I. Spectral scheme*, *MNRAS* **491** (2020) 993 [1909.12840].

[24] G. Winner, C. Pfrommer, P. Girichidis and R. Pakmor, *Evolution of cosmic ray electron spectra in magnetohydrodynamical simulations*, *MNRAS* **488** (2019) 2235 [1903.01467].

PoS(ICRC2021)665